Available online at www.sciencedirect.com
ScienceDirect
Journal of Computational Physics 227 (2008) 6821–6845
JOURNAL OF COMPUTATIONAL PHYSICS
www.elsevier.com/locate/jcp

Differential equation based constrained reinitialization for level set methods

Daniel Hartmann *, Matthias Meinke, Wolfgang Schröder

Institute of Aerodynamics, RWTH Aachen University, Wüllnerstr. 5a, 52062 Aachen, Germany

Received 16 July 2007; received in revised form 29 January 2008; accepted 26 March 2008
Available online 11 April 2008

Abstract

A partial differential equation based reinitialization method is presented in the framework of a localized level set method. Two formulations of the new reinitialization scheme are derived. These formulations are modifications of the partial differential equation introduced by Sussman et al. [M. Sussman, P. Smereka, S. Osher, A level set approach for computing solutions to incompressible two-phase flow, J. Comput. Phys. 114 (1994) 146–159] and, in particular, improvements of the second-order accurate modification proposed by Russo and Smereka [G. Russo, P. Smereka, A remark on computing distance functions, J. Comput. Phys. 163 (2000) 51–67]. The first formulation uses the least-squares method to explicitly minimize the displacement of the zero level set within the reinitialization. The overdetermined problem, which is solved in the first formulation of the new reinitialization scheme, is reduced to a determined problem in another formulation such that the location of the interface is locally preserved within the reinitialization. The second formulation is derived by systematically minimizing the number of constraints imposed on the reinitialization scheme. For both systems, the resulting algorithms are formulated in a three-dimensional frame of reference and are remarkably simple and efficient. The new formulations are second-order accurate at the interface when the reinitialization equation is solved with a first-order upwind scheme and do not diminish the accuracy of high-order discretizations of the level set equation. The computational work required for all components of the localized level set method scales with $\mathcal{O}(\mathcal{N})$. Detailed analyses of numerical solutions obtained with different discretization schemes evidence the enhanced accuracy and the stability of the proposed method, which can be used for localized and global level set methods.

Keywords: Localized level set method; Reinitialization; *G* equation; Distance function; Eikonal equation

1. Introduction

Level set methods have found various applications in which discontinuities in physical properties play an essential role and can be described by the propagation of an interface. Recent applications in computational physics concern turbulent premixed combustion [1,2], two-phase flows [3,4], and crystal growth [5]. In com-

* Corresponding author. Tel.: +49 241 80 90396; fax: +49 241 80 92257.
E-mail address: office@aia.rwth-aachen.de (D. Hartmann).

0021-9991/$ - see front matter © 2008 Elsevier Inc. All rights reserved.
doi:10.1016/j.jcp.2008.03.040

bustion, the idea of tracking a propagating surface to theoretically describe the front of a premixed flame was introduced by Markstein [6]. Later the derived equation became known as the G equation, which is formally equivalent to the level set equation. The numerical foundation of level set methods was established by Osher and Sethian [7].

The interface is commonly represented by the zero level set ϕ_0 bounding a region $\Omega^+ \subset R^n$ and separating $\Omega^- \subset R^n$ from Ω^+. It is embedded in the n-dimensional scalar level set function $\phi = \phi(\mathbf{x}, t)$,

$$\phi_0 = \{(\mathbf{x}, t) : \phi(\mathbf{x}, t) = 0\}, \quad \mathbf{x} \in R^n, \ t \in R^+. \tag{1}$$

For $n = 3$, let the components of the coordinate vector be denoted by $\mathbf{x} = (x, y, z)^{\mathrm{T}}$. The level set function ϕ can be any Lipschitz continuous function with the properties

$$\begin{cases} \phi > 0 & \text{for } \mathbf{x} \in \Omega^+, \\ \phi = 0 & \text{for } \mathbf{x} \in \phi_0, \\ \phi < 0 & \text{for } \mathbf{x} \in \Omega^-. \end{cases} \tag{2}$$

The motion of the zero level set ϕ_0 is governed by the extension velocity $\mathbf{f} = \mathbf{f}(\mathbf{x}, t)$,

$$\mathbf{f} = \mathbf{v} + s\mathbf{n} \tag{3}$$

with the components $\mathbf{f} = (f_x, f_y, f_z)^{\mathrm{T}}$. It comprises the advection by an underlying flow velocity field $\mathbf{v} = \mathbf{v}(\mathbf{x}, t)$ and the propagation of the front relative to the flow field in the normal direction to ϕ_0 by s. The normal direction is defined by the outward normal vector

$$\mathbf{n} = -\frac{\nabla\phi}{|\nabla\phi|} \tag{4}$$

pointing into Ω^-, where $\nabla = (\partial_x, \partial_y, \partial_z)^{\mathrm{T}}$ denotes the vector operator of spatial derivatives. The local speed of propagation s may be induced by several effects such as curvature [7] and, in the case of premixed combustion, the flame propagation into the unburnt gas. A great advantage of level set methods is geometric quantities such as the curvature

$$\mathfrak{C} = \nabla \cdot \mathbf{n} \tag{5}$$

to be readily obtained. The fundamental level set equation can be written

$$\partial_t\phi + \mathbf{f} \cdot \nabla\phi = 0 \tag{6}$$

or in terms of the normal velocity $f_n = -\mathbf{f} \cdot \mathbf{n}$

$$\partial_t\phi + f_n|\nabla\phi| = 0. \tag{7}$$

At $f_n = 1$, Eq. (7) is a Hamilton–Jacobi equation. Besides the accurate and efficient solution of the Hamilton–Jacobi type Eqs. (6) and (7), for which methods are reported in the literature [8,9], the reinitialization of the level set function ϕ is an important issue in level set methods having a substantial impact on the accuracy and the efficiency of the overall solution method.

1.1. Reinitialization of the level set function

In general, the formulation of Eq. (6) permits an arbitrary, sufficiently smooth function ϕ with the properties given in (2). However, solving Eq. (6) moves the zero level set ϕ_0 correctly, but may perturb the level set function near ϕ_0 [10,11], i.e., it may cause very large or small gradients. To alleviate this difficulty, it was proposed in [10,11] to replace the arbitrary level set function by a well behaved function and initialize ϕ into a signed distance function, which is the unique viscosity solution of the Eikonal equation

$$|\nabla\phi| = 1 \tag{8}$$

anchored at ϕ_0. However, once initialized into such a signed distance function, the level set function ϕ usually does not retain this property under the evolution of Eq. (6) and needs to be reinitialized at regular time intervals. The most straightforward but inefficient reinitialization technique is to directly compute the mini-

mum distance of each point from the zero level set, requiring a computational work of the order $\mathcal{O}(\mathcal{N}^2)$, with $\mathcal{N}$ being the number of cells. A more efficient and simpler approach is to use a partial differential equation to iteratively reinitialize the level set function. Sussman et al. [10] reformulate the Eikonal equation (8) as an evolution equation in artificial time τ

$$\partial_\tau \phi^v + S(\tilde{\phi})(|\nabla \phi^v| - 1) = 0, \tag{9}$$

which can be rewritten as a nonlinear hyperbolic equation

$$\partial_\tau \phi^v + \mathbf{w}(\phi^v) \cdot \nabla \phi^v = S(\tilde{\phi}), \tag{10}$$

where $\mathbf{w}(\phi^v) = S(\tilde{\phi}) \frac{\nabla \phi^v}{|\nabla \phi^v|}$ and the superscript v denotes the discrete pseudo-time step. The quantity $S(\tilde{\phi})$ is a smoothed sign function of the perturbed level set function $\tilde{\phi} = \tilde{\phi}(\mathbf{x}, \tau = 0)$ being defined as

$$S(\tilde{\phi}) = \frac{\tilde{\phi}}{\sqrt{\tilde{\phi}^2 + \epsilon^2}}, \tag{11}$$

where ϵ is a smoothing parameter. Analytically, Eqs. (9) and (10) yield for $\tau \to \infty$ the unique viscosity solution of the Eikonal equation correcting the perturbed level set function $\tilde{\phi}$ to become a signed distance function and keep the zero level set invariant because $S(\tilde{\phi}_0) = 0$. However, since in a discrete representation of $\tilde{\phi}$ hardly any computational points coincide with $\tilde{\phi}_0$, the location of the zero level set has to be defined by interpolating neighboring points. It has been emphasized by several authors [4,12] that solving the discretized version of Eq. (9) considerably displaces the zero level set and thus may lead to substantial errors due to the reinitialization. A number of approaches were taken to remedy this problem [4,12]. It was pointed out in [8] that the modification proposed in [4] prevents a steady-state solution of the reinitialization equation (9) and leads to oscillations of the zero level set within the reinitialization procedure. It will be shown in this paper that the original second-order method of Russo and Smereka [12] also produces oscillations of the zero level set.

1.2. Objectives

Ultimately, numerical methods used for the reinitialization of the level set function should be designed based on the following criteria:

(1) The ϕ_0 iso-surface is kept invariant by the reinitialization.
(2) The level set function satisfies a signed distance function, i.e., $|\nabla \phi| = 1$, which is anchored at ϕ_0.
(3) The schemes can be efficiently applied to large-scale problems.

Regarding these criteria two formulations of a new partial differential equation based reinitialization scheme are derived. The first formulation is based on the least-squares method which minimizes the unwanted displacement of the interface within the reinitialization. The overdetermined problem, which is solved in this first formulation of the reinitialization, is reduced to a determined problem in a second formulation such that the location of the interface is preserved within the reinitialization. The second formulation is derived by minimizing the number of constraints imposed on the reinitialization scheme in the first formulation. The new formulations are modifications of the differential equation based methods introduced in [10] and modified in [12] and are remarkably simple and efficient.

This paper is organized as follows. After a brief description of the localized level set method in Section 2, two formulations of a new reinitialization method are derived in Section 3. Results of two-dimensional computations are given in Section 4, before the findings of the present paper are summarized in Section 5.

2. Level set formulation

For the sake of a simple description of the algorithms, a computational domain Ω is considered with a cell-centered discretization on a uniform mesh using a constant spacing $\Delta_{\mathbf{x}} = \Delta_\zeta$, $\zeta = \{x, y, z\}$, in the x, y and z direction, respectively. All methods described below are also suitable for curvilinear coordinates. The cells

in Ω are denoted by $C_{i,j,k}$, where the subscripts indicate their discrete location in the computational grid. Furthermore, the subset Γ of cells which are adjacent to the zero level set is defined by

$$\Gamma = \left\{ C_{i,j,k} : \left(\Pi^{i,j,k}_{i',j,k}\phi \leqslant 0 \right) \vee \left(\Pi^{i,j,k}_{i,j',k}\phi \leqslant 0 \right) \vee \left(\Pi^{i,j,k}_{i,j,k'}\phi \leqslant 0 \right) \right\} \tag{12}$$

for any combination of integers $i' \in \{i+1, i-1\}, j' \in \{j+1, j-1\}, k' \in \{k+1, k-1\}$, with $\Pi^{i,j,k}_{i',j,k}\phi = \phi_{i,j,k}\phi_{i',j,k}$. That is, all cells in Γ are located within a distance Δ_x from the zero level set, Fig. 1.

The computational costs of solving the level set Eq. (6) can be reduced by orders of magnitude when the level set method is localized, i.e., a solution is sought only in a small region around the zero level set, while all other areas are assigned a constant value indicating the location in Ω^+ or Ω^- [13,14]. In this paper, we consider a localized computational domain $\Omega_\phi \subset \Omega$ moving along with the zero level set. All cells outside Ω_ϕ are discarded and the level set algorithms are localized as proposed in [13], such that the computational costs of the overall level set method scale with $\mathcal{O}(\mathcal{N})$. Let $\mathcal{B}$ designate the subset of cells $C_{i,j,k}$ which are used in the localized solution of Eq. (6) forming a narrow band around ϕ_0 bounded by the boundary cells $\widehat{C}_{i,j,k} \in \partial\mathcal{B}$. Let us furthermore define $\partial\mathcal{B} \cap \Omega_\phi = \emptyset$ such that boundary cells are outside of and adjacent to Ω_ϕ, Fig. 1. $\mathcal{B}$ is created using an efficient marching algorithm, which is based on neighbor relations. The Cartesian flow solver underlying the present level set method is based on a hierarchical quadtree/octree data structure such that all neighbor information can be directly accessed [15]. The narrow band $\mathcal{B}$ is regenerated before each reinitialization step, while the subset Γ is updated after each time step.

2.1. Discretization

The level set equation (6) is integrated in time with a 3-step third-order accurate TVD Runge–Kutta scheme [16] denoted by RK_3,

$$\begin{cases} \phi^{(0)} = \phi^w, \\ \phi^{(k)} = \alpha_k \phi^{(0)} + \beta_k \phi^{(k-1)} - \gamma_k \Delta t L(\phi^{(k-1)}), \\ \phi^{w+1} = \phi^{(N)}, \end{cases} \tag{13}$$

where $N = 3$ and the coefficients $\boldsymbol{\alpha} = (0, \frac{3}{4}, \frac{1}{3})$, $\boldsymbol{\beta} = (1, \frac{1}{4}, \frac{2}{3})$ and $\boldsymbol{\gamma} = (1, \frac{1}{4}, \frac{2}{3})$ are used. The superscript k denotes the Runge–Kutta step, while the superscript w counts the time steps Δt. The operator $L(\phi)$ denotes the numerical approximation of the term $\mathbf{f} \cdot \nabla\phi$ in Eq. (6), which is specified in the following. To spatially discretize the level set equation, unlimited third- and fifth-order upstream central schemes denoted by UC_3 and UC_5 are

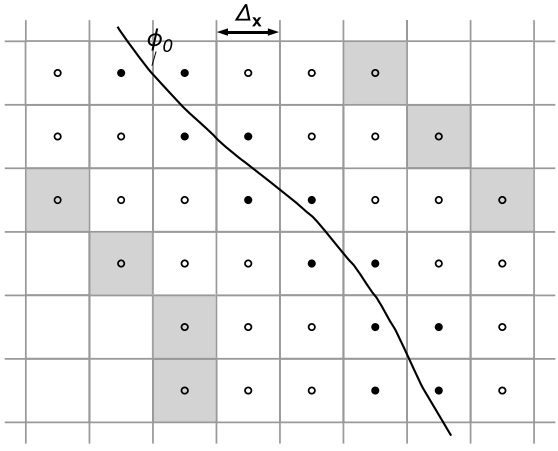

Fig. 1. $\mathcal{B}$ and Ω_ϕ in the localized level set method. In this example, $\mathcal{B}$ extends four cells on either side of the zero level set. Circles denote cell centers of internal and boundary cells in $\mathcal{B}$; shaded cells are boundary cells in $\partial\mathcal{B}$; Ω_ϕ consists of internal cells only; dots denote cells in Γ.

used, respectively. Both schemes are investigated in [8] and shown to give excellent results. Using UC_5 the discrete upwind-biased spatial derivatives read in the x direction

$$\begin{cases} D^{x,L}_{i,j,k} = \dfrac{1}{60\Delta_{\mathbf{x}}}\Big(-2\phi_{i-3,j,k} + 15\phi_{i-2,j,k} - 60\phi_{i-1,j,k} + 20\phi_{i,j,k} + 30\phi_{i+1,j,k} - 3\phi_{i+2,j,k}\Big), \\ D^{x,R}_{i,j,k} = \dfrac{1}{60\Delta_{\mathbf{x}}}\Big(2\phi_{i+3,j,k} - 15\phi_{i+2,j,k} + 60\phi_{i+1,j,k} - 20\phi_{i,j,k} - 30\phi_{i-1,j,k} + 3\phi_{i-2,j,k}\Big), \end{cases} \tag{14}$$

where $\partial_x\phi|^{L/R}_{i,j,k} = D^{x,L/R}_{i,j,k} + \mathcal{O}(\Delta^5_{\mathbf{x}})$. With UC_3, the derivatives in the x direction are approximated by

$$\begin{cases} D^{x,L}_{i,j,k} = \dfrac{1}{6\Delta_{\mathbf{x}}}\Big(\phi_{i-2,j,k} - 6\phi_{i-1,j,k} + 3\phi_{i,j,k} + 2\phi_{i+1,j,k}\Big), \\ D^{x,R}_{i,j,k} = \dfrac{1}{6\Delta_{\mathbf{x}}}\Big(-\phi_{i+2,j,k} + 6\phi_{i+1,j,k} - 3\phi_{i,j,k} - 2\phi_{i-1,j,k}\Big), \end{cases} \tag{15}$$

where $\partial_x\phi|^{L/R}_{i,j,k} = D^{x,L/R}_{i,j,k} + \mathcal{O}(\Delta^3_{\mathbf{x}})$. Likewise derivatives with respect to the y and z direction are obtained by exchanging the respective subscripts. Let us define $D^{x,\pm}_{i,j,k} \equiv D^{x,L}_{i,j,k} \pm D^{x,R}_{i,j,k}$ and introduce the vector operator $\mathfrak{D}^{\pm}_{i,j,k} = (D^{x,\pm}_{i,j,k}, D^{y,\pm}_{i,j,k}, D^{z,\pm}_{i,j,k})^{\mathrm{T}}$. Then, $L(\phi)$ can be computed by

$$L(\phi_{i,j,k}) = \frac{1}{2}\left\{\left(\sum_{\zeta}|f_\zeta|\mathbf{e}_\zeta\right)\cdot\mathfrak{D}^{+}_{i,j,k} + \mathbf{f}\cdot\mathfrak{D}^{-}_{i,j,k}\right\}, \quad \zeta = \{x,y,z\}, \tag{16}$$

where the summation is over all spatial directions, $\mathbf{e}_\zeta$ is the unit vector in the ζ direction and $\mathbf{f}$ is evaluated on the cell $C_{i,j,k}$.

Localized level set methods are known to have stability problems at the boundary [13], which can be avoided by introducing the Heaviside function

$$c(\mathbf{x}) = \begin{cases} 1 & \text{if } \mathbf{x} \in \Omega_\phi, \\ 0 & \text{otherwise} \end{cases} \tag{17}$$

to obtain

$$\partial_t\phi + c(\mathbf{x})\mathbf{f}\cdot\nabla\phi = 0 \tag{18}$$

in conjunction with a reduced-order discretization near $\partial\mathcal{B}$. Unless the UC_5 stencil lies completely in $\mathcal{B}$, UC_3 is used near $\partial\mathcal{B}$ or a first-order upwind scheme if the UC_3 stencil contains a cell which is not in $\mathcal{B}$. A likewise reduction applies when UC_3 is used as base scheme. Using Eq. (17), cells on $\partial\mathcal{B}$ are not updated, such that the localized solution of the level set function evolves based on data in $\mathcal{B}$ only.

A more sophisticated form of the cut-off function (17) is proposed in [13]. However, the simple formulation (17) in conjunction with the reduced-order discretization near $\partial\mathcal{B}$ performed well in all test cases presented in Section 4.

3. Reinitialization of the level set function

A major difficulty in partial differential equation based reinitialization methods is to avoid the displacement of the zero level set within the reinitialization. It is evident that finite-order approximations of these equations cause these displacements in the general multi-dimensional case, if a solution to $|\nabla\phi| = 1$ is sought without further constraints. A major drawback of the differential reinitialization equation (9) is that the zero level set is considerably displaced and that this displacement may increase with an increasing number of iterations. Russo and Smereka [12] improve the original Hamilton–Jacobi formulation (9) by Sussman et al. [10] by discretizing Eq. (9) such that the stencils use information of only one side of the zero level set. Furthermore, it is shown that, unlike in the original formulation, the unwanted displacement of the zero level set in the modified reinitialization scheme is independent of the number of iterations. Their modified formulation reads

$$\phi^{v+1}_{i,j,k} = \begin{cases} \phi^{v}_{i,j,k} - \frac{\Delta\tau}{\Delta_{\mathbf{x}}}\left(\operatorname{sgn}(\tilde{\phi}_{i,j,k})|\phi^{v}_{i,j,k}| - d_{i,j,k}\right) & \text{if } C_{i,j,k} \in \Gamma, \\ \phi^{v}_{i,j,k} - \Delta\tau\ \operatorname{sgn}(\tilde{\phi}_{i,j,k})(|\nabla\phi^{v}_{i,j,k}| - 1) & \text{otherwise,} \end{cases} \tag{19}$$

where $\tilde{\phi}$ denotes the level set function before the reinitialization, i.e., $\tilde{\phi} = \phi^{v=0}$ and

$$d_{i,j,k} = \frac{\tilde{\phi}_{i,j,k}}{\left(\left[\partial_x\tilde{\phi}_{i,j,k}\right]^2 + \left[\partial_y\tilde{\phi}_{i,j,k}\right]^2 + \left[\partial_z\tilde{\phi}_{i,j,k}\right]^2\right)^{1/2}} \tag{20}$$

is the target value of the level set function on $C_{i,j,k} \in \Gamma$ approximating the signed distance function. As noted in [12], an alternative to iteratively determining the level set function on the cells in Γ is to directly update $\phi_{i,j,k} = d_{i,j,k}\ \forall C_{i,j,k} \in \Gamma$. The iterative and the direct update were tested in the present investigation and no difference in the stability and the rate of convergence was found, which is why the direct update is used in this paper. In both cases, the CFL stability condition requires $\Delta\tau < \Delta_{\mathbf{x}}$. A central difference scheme is proposed in [12] to evaluate the discrete derivatives $[\partial_\zeta\tilde{\phi}_{i,j,k}],\ \zeta = \{x, y, z\}$, in Eq. (20). As indicated in Fig. 2, this central scheme results in oscillations of the interface location in the solutions, which can be stabilized using an upwind discretization across the zero level set instead. This discretization reads in general form e.g. for the x direction

$$[\partial_x\tilde{\phi}_{i,j,k}] = \frac{\tilde{\phi}^{+}_{(i,j,k)} - \tilde{\phi}^{-}_{(i,j,k)}}{\max\left(x^{+}_{(i,j,k)} - x^{-}_{(i,j,k)}, \epsilon_{\mathbf{x}}\right)}, \tag{21a}$$

where $\epsilon_{\mathbf{x}} = \frac{\Delta_{\mathbf{x}}}{1000}$ and for $\xi = \{\tilde{\phi}, x\}$

$$\xi^{\pm}_{(i,j,k)} = \begin{cases} \xi_{i,j,k} & \text{if } C_{i\pm1,j,k} \notin \Gamma \vee ((A) \wedge (B)), \\ \xi_{i\pm1,j,k} & \text{otherwise,} \end{cases} \tag{21b}$$

where the conditions (A) and (B) read with $\Delta^{+}_{i,j,k}\phi = \phi_{i+1,j,k} - \phi_{i,j,k}$ and $\Delta^{-}_{i,j,k}\phi = \phi_{i,j,k} - \phi_{i-1,j,k}$

$$\begin{cases} (A) & \text{if } \left(\Pi^{i+1,j,k}_{i-1,j,k}\phi < 0\right) \wedge \left(|\Delta^{\pm}_{i,j,k}\phi + \epsilon_{\mathbf{x}}| < |\Delta^{\mp}_{i,j,k}\phi|\right), \\ (B) & \text{if } \left(\Delta^{+}_{i,j,k}\phi\Delta^{-}_{i,j,k}\phi < 0\right) \vee \left(\Pi^{i-1,j,k}_{i-2,j,k}\phi < 0\right) \vee \left(\Pi^{i+1,j,k}_{i+2,j,k}\phi < 0\right). \end{cases} \tag{21c}$$

The conditions (A) and (B) are formulated to take into account cases in which multiple interfaces are close to each other and about to coalesce, see e.g. problem 3 in Section 4.2.3. In most other scenarios, either condition (A) or (B) is not fulfilled such that Eq. (21) reduces to a simple upwind/center difference scheme utilizing only cells in Γ. Discretization schemes for the y and the z directions are obtained by exchanging the corresponding

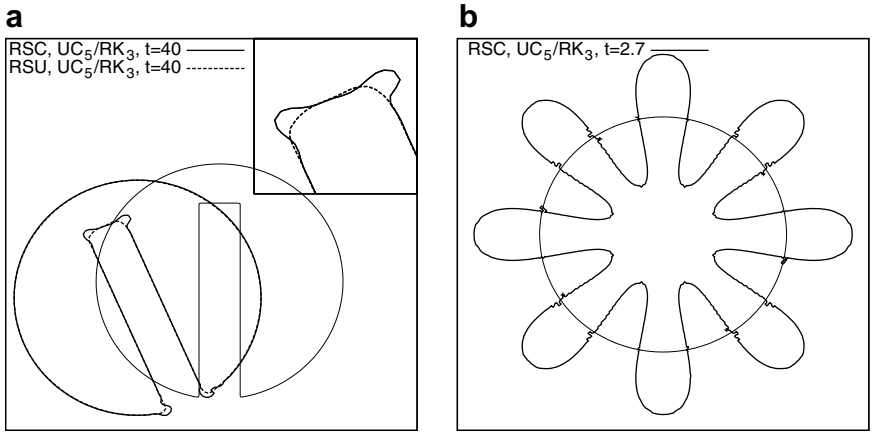

Fig. 2. Comparison of UC_5/RK_3 solutions using the reinitialization schemes RSC and RSU: (a) rotation of a slotted disk; (b) propagation of a circular zero level set using RSC. The level set function is reinitialized after each time step. The solutions clearly illustrate the kinks produced by RSC, while RSU is stable (see also Fig. 15). The thin lines show the initial zero level set. Details of the test cases are given in Sections 4.2.1 and 4.2.2.

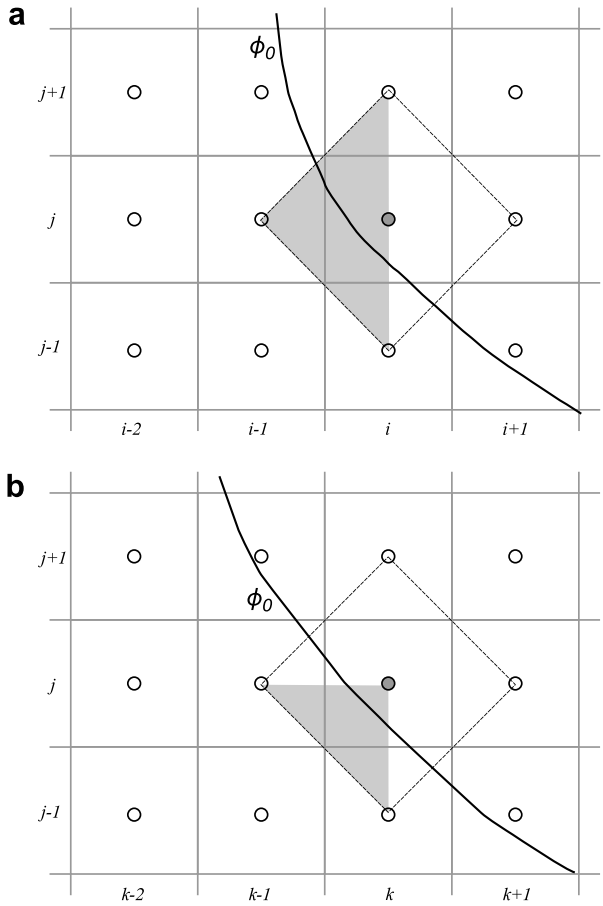

Fig. 3. Illustration of the stencils to discretize Eq. (20) for different reinitialization schemes: (a) x–y plane at $z = k$; (b) z–y plane at $x = i$. Circles denote cell centers; the diamond-shaped areas surrounded by dashed lines illustrate the central difference stencil used in [12] (RSC) for the cell marked by the shaded circle; the upwind discretization stencil, Eq. (21), used in RSU, CR-1 and CR-2 is given by the shaded areas.

subscripts. In the following, the Russo–Smereka scheme (19) is denoted by RSC when used in conjunction with a central discretization scheme and is denoted by RSU when discretized by the upwind scheme given by Eq. (21). In Fig. 3, the stencils for the RSC and RSU schemes are illustrated.

3.1. Constrained reinitialization scheme

We now turn to present two formulations of a new reinitialization scheme which are derived by explicitly imposing the zero-displacement constraint on the zero level set. Whereas they are formally closely connected, the philosophy behind these formulations is different. The formulations are modifications of the scheme introduced by Sussman et al. [10], Eq. (9) and do improve the modification of this scheme proposed by Russo and Smereka [12]. The first formulation denoted by CR-1 is based on the least-squares method and is formulated to minimize the displacement of the zero level set within the reinitialization. The second formulation denoted by CR-2 is derived by systematically minimizing the number of constraints imposed on the scheme CR-1. The overdetermined problem which is solved in CR-1 is reduced to a determined problem such that the location of the interface can be preserved within the reinitialization.

Considering a cell in Γ, the difference between the formulations can be briefly summarized as follows. In the first formulation, the level set function on this cell is determined such that the accumulated displacement of the zero level set at all points which can be identified by linear interpolation in the Cartesian space directions is minimized. In the general multi-dimensional case, multiple such points exist such that the zero level set cannot

be restrained. The essence of the second formulation is to represent this cloud of points by a single point in ϕ_0, to which the zero level set can be anchored. The level set function on the considered cell is in the second formulation determined such that this single point remains invariant.

3.1.1. Formulation CR-1

In general, reinitialization methods can be judged by their capability to

- modify the level set function such that $|\nabla\phi| = 1$ is satisfied,
- keep the ϕ_0 iso-surface invariant.

While the first criterion is relevant for all cells in $\mathcal{B}$, the second condition is important only for the cells in Γ. Both criteria can be fulfilled analytically, but one usually faces an overdetermined problem in the discrete version of the level set function in multi-dimensional space such that a solution which exactly meets both criteria cannot be obtained. Hence, for the cells in Γ, a reinitialization scheme which minimizes the deviation from the above stated criteria is sought. Using linear interpolation to determine the location of the zero level set, these errors can formally be written

$$\begin{cases} (\varepsilon_{i,j,k})_0 = \left([\partial_x \phi_{i,j,k}]^2 + [\partial_y \phi_{i,j,k}]^2 + [\partial_z \phi_{i,j,k}]^2 \right)^{1/2} - 1, \\ (\varepsilon_{i,j,k})_\alpha = \phi_{i,j,k} - r^{i,j,k}_{(i,j,k)_\alpha} \phi_{(i,j,k)_\alpha}, \quad C_{(i,j,k)_\alpha} \in \mathcal{S}_{i,j,k}, \end{cases} \tag{22}$$

where $r^{i,j,k}_{(i,j,k)_\alpha} = \frac{\tilde{\phi}_{i,j,k}}{\tilde{\phi}_{(i,j,k)_\alpha}}$ and $\mathcal{S}_{i,j,k}$ contains the neighbor cells of $C_{i,j,k}$ across the ϕ_0 iso-surface, i.e.,

$$\mathcal{S}_{i,j,k} = \{ C_{(i,j,k)_\alpha} : \phi_{i,j,k} \phi_{(i,j,k)_\alpha} < 0 \}. \tag{23}$$

The quantity $(\varepsilon_{i,j,k})_0$ is the deviation from $|\nabla\phi| = 1$ and $(\varepsilon_{i,j,k})_\alpha$ can be considered a measure of the interface displacement on the line connecting the cell centers of $C_{i,j,k}$ and $C_{(i,j,k)_\alpha}$. Furthermore, let $M_{i,j,k}$ denote the number of cells in $\mathcal{S}_{i,j,k}$ such that $\alpha = \{1, \ldots, M_{i,j,k}\}$. Summing up the squared errors weighted by the quantity $\delta_{\alpha'}$ yields the least-squares function $\mathcal{L}$

$$\mathcal{L}_{i,j,k} = \sum_{\alpha'=0}^{M_{i,j,k}} \delta_{\alpha'} (\varepsilon_{i,j,k})^2_{\alpha'}. \tag{24}$$

In the case depicted in Fig. 4, $M_{i,j,k} = 3$ and $\mathcal{S}_{i,j,k} = \{C_{i-1,j,k}, C_{i,j-1,k}, C_{i,j,k-1}\}$. To find the minimum error, $\mathcal{L}_{i,j,k}$ is differentiated with respect to the $M_{i,j,k} + 1$ unknowns, the derivatives are set 0 and the resulting system of $M_{i,j,k} + 1$ equations is solved. For example, the equation resulting from differentiating with respect to $\phi_{i,j,k}$ reads

$$\partial_{\phi_{i,j,k}} \mathcal{L}_{i,j,k} = \partial_{\phi_{i,j,k}} \delta_0 (\varepsilon_{i,j,k})^2_0 + 2 \left(\sum_{\alpha=1}^{M_{i,j,k}} \delta_\alpha (\varepsilon_{i,j,k})_\alpha \right) = 0. \tag{25}$$

In Eq. (25) and the corresponding equations for the derivatives with respect to $\phi_{(i,j,k)_\alpha}, \alpha = \{1, \ldots, M_{i,j,k}\}$, the first term on the right-hand side, i.e., the derivative of $(\varepsilon_{i,j,k})^2_0$, is nonlinear such that Eq. (25) and the corresponding equations are difficult to solve analytically. Iterative solution schemes can be derived but introduce complexity. However, provided the level set function has been reinitialized via Eq. (20) into a signed distance function in Γ, $(\varepsilon_{i,j,k})_0$ may be assumed very small and the weighting

$$\delta_{\alpha'} = \begin{cases} 0, & \alpha' = 0, \\ 1, & \alpha' \geqslant 1 \end{cases} \tag{26}$$

can be introduced into Eq. (25), which then readily allows to determine $\phi_{i,j,k}$. To be consistent with Eq. (19), this equation is written in terms of the signed distance

$$\tilde{d}_{i,j,k} = \frac{1}{M_{i,j,k}} \sum_{\alpha=1}^{M_{i,j,k}} r^{i,j,k}_{(i,j,k)_\alpha} d_{(i,j,k)_\alpha}, \tag{27}$$

which can be introduced into the scheme (19) by setting $d_{i,j,k} = \tilde{d}_{i,j,k}$ or used to directly update the level set function by $\phi_{i,j,k} = \tilde{d}_{i,j,k}$. Since Eq. (27) is an equation for the signed distance on the cell $C_{i,j,k}$, there is no need to precom-

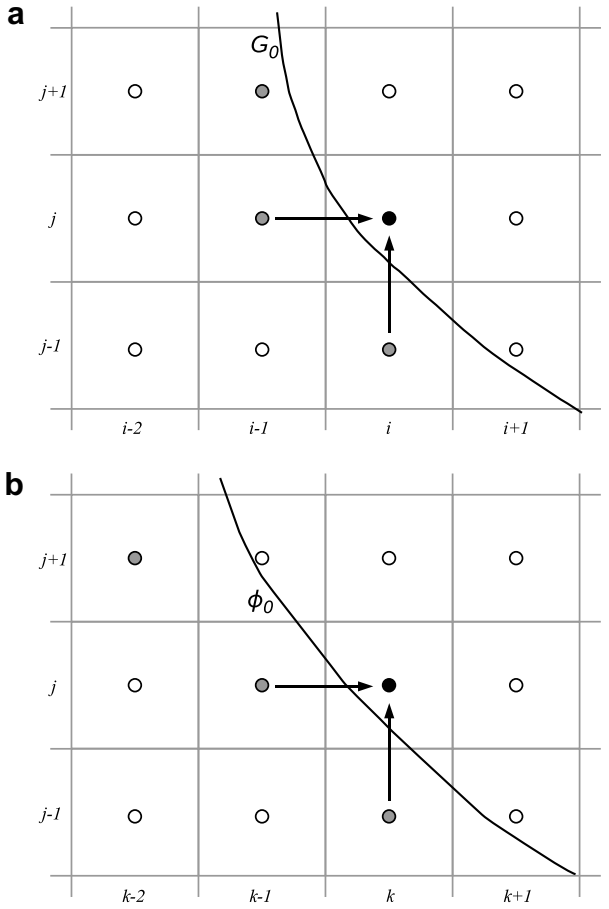

Fig. 4. Illustration of the ϕ_0 iso-surface in a three-dimensional Cartesian frame of reference: (a) x–y plane at $z = k$; (b) z–y plane at $x = i$. Circles denote cell centers; shaded circles denote the set $\mathcal{R}$, i.e., those cells to which step 1 is applied in CR-1 and CR-2. Arrows pointing towards $C_{i,j,k}$ marked by the filled circle indicate the set $\mathcal{S}_{i,j,k}$ containing the cells, which are used in Eqs. (27) and (36), respectively.

pute this distance using Eq. (20). Considering the example depicted in Fig. 4, the signed distance function d needs to be precomputed only on the cells in $\mathcal{S}_{i,j,k}$. Hence, a 2-step correction scheme is obtained, which in the first step computes the signed distance function on the cells in $\mathcal{S}_{i,j,k}$ using Eq. (20) and in the second step uses Eq. (27) to compute $\tilde{d}_{i,j,k}$ on all other cells in Γ. Both steps are performed only once and sequentially, such that the $d_{(i,j,k)_\alpha}$ required in Eq. (27) are available from the first step and Eq. (27) is thus explicit. Hence, no iterations between the two steps are necessary to obtain an estimate of $d_{i,j,k}$ on cells at the zero level set.

As illustrated in Fig. 5 for the one-dimensional case, applying the second step to $C_{i,j,k}$ gives exactly the same result as reinitializing the level set function using Eqs. (20) and (21) on all cells in Γ. In this limiting case it can thus be considered a redistancing constraint. In the general multi-dimensional case, the level set function is allowed to deviate from $|\nabla\phi| = 1$ by the introduction of $\delta_0 = 0$. Then, the second reinitialization step via Eq. (27) seeks to minimize the displacement of the zero level set. However, the results of our numerical experiments presented in Section 4 evidence that the first step, i.e., the reinitialization of the level set function into a signed distance function on only one side of the zero level set, is sufficient to obtain a close approximation of the signed distance function on all cells if Eq. (27) is used on the other side of the interface. In fact, the approximation of the signed distance function using CR-1 is as accurate as if the reinitialization into a signed distance function is explicitly performed on all cells via the scheme RSU.

Preliminary numerical experiments suggest that the cells on which steps 1 and 2 are executed should be determined according to the local curvature. Essentially, the sets $\mathcal{S}_{i,j,k}$ should contain as many cells as possible. Accordingly, let Γ be divided into two subsets $\mathcal{R}$ and $\mathcal{C}$ such that

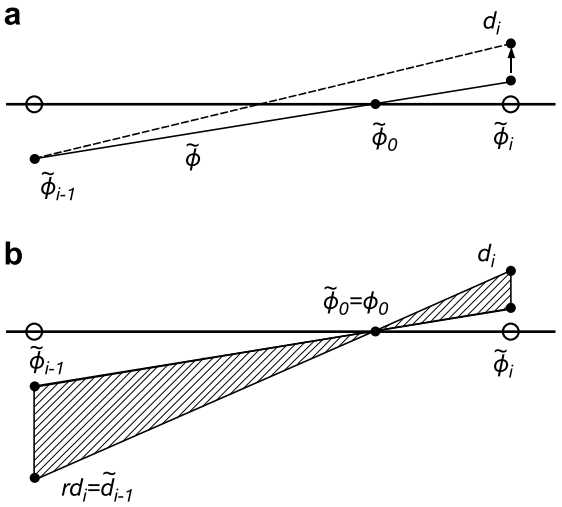

Fig. 5. Illustration of the 2-step correction in the schemes CR-1 and CR-2 for the one-dimensional case: (a) step 1: reinitialization of $\phi_i = d_i$, Eqs. (20) and (21); (b) step 2: reinitialization of $\phi_{i-1} = \tilde{d}_{i-1} = r_i^{i-1} d_i$, Eqs. (27) and (36), using explicitly the constraint that $\phi_0 = \tilde{\phi}_0$. For the one-dimensional case, step 2 is equivalent to executing step 1 for ϕ_{i-1} and $\phi_0 = \tilde{\phi}_0$.

$$\begin{cases} \mathcal{R} = \{C_{i,j,k} \in \Gamma : \mathfrak{C}_{i,j,k}\tilde{\phi}_{i,j,k} > 0 \vee (\mathfrak{C}_{i,j,k} = 0 \wedge \tilde{\phi}_{i,j,k} > 0)\}, \\ \mathcal{C} = \{\Gamma \setminus \mathcal{R}\}, \end{cases} \tag{28}$$

where the curvature $\mathfrak{C}_{i,j,k}$, Eq. (5), is computed on the cell $C_{i,j,k}$. Then, $\mathcal{R} = \bigcup \mathcal{S}_{i,j,k}$ and the overall reinitialization scheme CR-1 can be summarized as follows:

Step 1. Compute the signed distance function on all cells in $\mathcal{R}$ using Eqs. (20) and (21).
Step 2. Apply Eq. (27) and set $d_{i,j,k} = \tilde{d}_{i,j,k}$ on all cells in $\mathcal{C}$.
Step 3. Update $\phi_{i,j,k} = d_{i,j,k}$ on all cells in Γ.
Step 4. Solve the reinitialization Eq. (9) to steady state on $C_{i,j,k} \in \{\mathcal{B} \setminus \Gamma\}$.

This scheme is very simple and of comparable computational costs as solving Eq. (9) for all cells or using the scheme (19). It updates the level set function on the cells in Γ in steps 1-3 before iteratively reinitializing all other cells in $\mathcal{B}$ using the original Eq. (9) proposed in [10]. Using a first-order spatial discretization and forward Euler integration in pseudo-time τ, Eq. (9) reads in its discretized form

$$\phi_{i,j,k}^{v+1} = \phi_{i,j,k}^{v} - \Delta\tau \frac{\tilde{\phi}_{i,j,k}}{|\tilde{\phi}_{i,j,k}|}(\mathcal{G}(D_\zeta^+\phi_{i,j,k}^v, D_\zeta^-\phi_{i,j,k}^v) - 1), \quad \zeta = \{x,y,z\}, \tag{29a}$$

where the pseudo-time step is $\Delta\tau = \frac{\Delta_{\mathbf{x}}}{4}$ and $\mathcal{G}$ is the Godunov Hamiltonian

$$\mathcal{G}(a,b,c,d,e,f) = \begin{cases} \sqrt{\max(a_+^2, b_-^2) + \max(c_+^2, d_-^2) + \max(e_+^2, f_-^2)} & \text{if } \tilde{\phi}_{i,j,k} \geqslant 0, \\ \sqrt{\max(a_-^2, b_+^2) + \max(c_-^2, d_+^2) + \max(e_-^2, f_+^2)} & \text{if } \tilde{\phi}_{i,j,k} < 0 \end{cases} \tag{29b}$$

with $a_+ = \max(a, 0)$ and $a_- = \min(a, 0)$ and

$$a \equiv D_x^-\phi_{i,j,k} = \frac{\phi_{i,j,k} - \phi_{i-1,j,k}}{\Delta_{\mathbf{x}}}, \quad b \equiv D_x^+\phi_{i,j,k} = \frac{\phi_{i+1,j,k} - \phi_{i,j,k}}{\Delta_{\mathbf{x}}},$$
$$c \equiv D_y^-\phi_{i,j,k} = \frac{\phi_{i,j,k} - \phi_{i,j-1,k}}{\Delta_{\mathbf{x}}}, \quad d \equiv D_y^+\phi_{i,j,k} = \frac{\phi_{i,j+1,k} - \phi_{i,j,k}}{\Delta_{\mathbf{x}}},$$
$$e \equiv D_z^-\phi_{i,j,k} = \frac{\phi_{i,j,k} - \phi_{i,j,k-1}}{\Delta_{\mathbf{x}}}, \quad f \equiv D_z^+\phi_{i,j,k} = \frac{\phi_{i,j,k+1} - \phi_{i,j,k}}{\Delta_{\mathbf{x}}}.$$

Eq. (29) constitutes a consistent and monotone discretization scheme of Eq. (9), which converges to the unique viscosity solution of the Eikonal equation [10].

3.1.2. Formulation CR-2

In this section, the derivation of the formulation CR-2 is presented. We start by executing step 1 of CR-1, i.e., the level set function is reinitialized using Eqs. (20) and (21) on all cells in $\mathcal{R}$. Step 2 of CR-1 is reformulated to give a relation which locally anchors the position of the zero level set. Consider again the cells $\mathcal{S}_{i,j,k}$ depicted in Fig. 4, which are reinitialized into a signed distance function in step 1. The center points of these cells span a polygon, which is depicted as the hatched triangle in Fig. 6. The perturbed level set function and the signed distance function can be interpolated to the center of this polygon using the second-order accurate interpolation operators $I_{(i,j,k)}\tilde{\phi}$ and $I_{(i,j,k)}d$ given by

$$I_{(i,j,k)}\tilde{\phi} = \frac{1}{M_{i,j,k}} \sum_{\alpha=1}^{M_{i,j,k}} \tilde{\phi}_{(i,j,k)_\alpha} \tag{30a}$$

and

$$I_{(i,j,k)}d = \frac{1}{M_{i,j,k}} \sum_{\alpha=1}^{M_{i,j,k}} d_{(i,j,k)_\alpha}, \tag{30b}$$

i.e., $I_{(i,j,k)}\tilde{\phi}$ and $I_{(i,j,k)}d$ evaluate the average of the corresponding variable values on the cells in $\mathcal{S}_{i,j,k}$. Using the interpolated values, we can show that the location of the zero level set remains locally fixed if the reinitialization scheme preserves the relation

$$\frac{d_{i,j,k}}{I_{(i,j,k)}d} = \frac{\tilde{\phi}_{i,j,k}}{I_{(i,j,k)}\tilde{\phi}}. \tag{31}$$

Consider the location of $\tilde{\phi}_0$ before the reinitialization and the location of ϕ_0 after the reinitialization on the line connecting $\mathbf{x}_{i,j,k}$ corresponding to the cell center of $C_{i,j,k}$ and $\mathbf{x}_{\mathcal{S}_{i,j,k}}$ corresponding to the center point of the polygon spanned by $\mathcal{S}_{i,j,k}$. Furthermore, let $\overline{\Delta_{\mathbf{x}}}$ be $\overline{\Delta_{\mathbf{x}}} = \mathbf{x}_{\mathcal{S}_{i,j,k}} - \mathbf{x}_{i,j,k}$. Using linear interpolation, the locations $\tilde{\mathbf{x}}_0$ of $\tilde{\phi}_0$ and $\mathbf{x}_0$ of ϕ_0 can be computed by

$$\tilde{\mathbf{x}}_0 = \mathbf{x}_{i,j,k} + \overline{\Delta_{\mathbf{x}}} \frac{\tilde{\phi}_{i,j,k}}{\tilde{\phi}_{i,j,k} - I_{(i,j,k)}\tilde{\phi}_{i,j,k}} \tag{32}$$

and

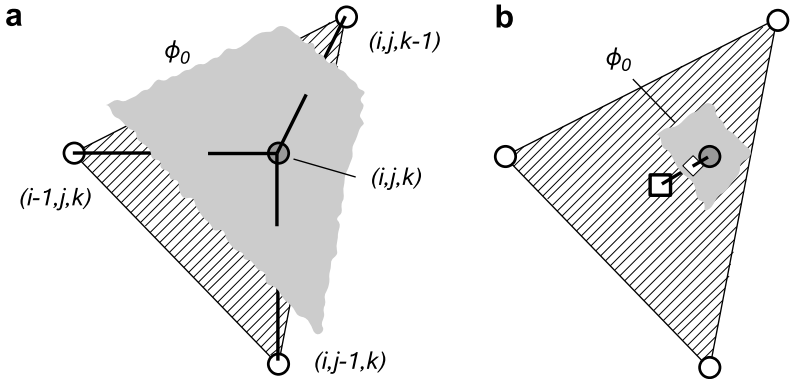

Fig. 6. Illustration of the determined problem in the scheme CR-2: (a) three-dimensional view of the problem; (b) reduced determined problem. Circles denote cell centers, the shaded circle denotes the cell $C_{i,j,k}$. The hatched areas illustrate the stencil of cells used to determine $d_{i,j,k}$ via Eq. (36). The square denotes the center of this stencil, to which d and ϕ are interpolated via Eq. (30). The open diamond marks the point to which the ϕ_0 iso-surface is anchored by the scheme.

$$\mathbf{x}_0 = \mathbf{x}_{i,j,k} + \overline{\Delta_{\mathbf{x}}} \frac{d_{i,j,k}}{d_{i,j,k} - I_{(i,j,k)} d_{i,j,k}}. \tag{33}$$

The condition $\mathbf{x}_0 = \tilde{\mathbf{x}}_0$ is satisfied if

$$\frac{1}{1 - \frac{I_{(i,j,k)}\tilde{\phi}}{\tilde{\phi}_{i,j,k}}} = \frac{1}{1 - \frac{I_{(i,j,k)}d}{d_{i,j,k}}}, \tag{34}$$

which is exactly fulfilled by Eq. (31).

Since $I_{(i,j,k)}\tilde{\phi}$ is determined before and $I_{(i,j,k)}d$ is determined after step 1, $d_{i,j,k}$ can be computed by rearranging Eq. (31) to obtain

$$d_{i,j,k} = \tilde{\phi}_{i,j,k} \frac{I_{(i,j,k)}d}{I_{(i,j,k)}\tilde{\phi}}, \tag{35}$$

which can be rewritten by substituting $I_{(i,j,k)}\tilde{\phi}$ and $I_{(i,j,k)}d$ and using $\tilde{d}_{i,j,k}$ to be consistent with Eq. (27),

$$\tilde{d}_{i,j,k} = \tilde{\phi}_{i,j,k} \frac{\sum_{\alpha=1}^{M_{i,j,k}} d_{(i,j,k)_\alpha}}{\sum_{\alpha=1}^{M_{i,j,k}} \tilde{\phi}_{(i,j,k)_\alpha}}. \tag{36}$$

It is clear that Eq. (36) exactly fulfills the constraint (31), see Fig. 5, such that the ϕ_0 iso-surface is fixed at the location of its intersection with the line connecting $\mathbf{x}_{i,j,k}$ and $\mathbf{x}_{\mathcal{S}_{i,j,k}}$, which is depicted as the open square in Fig. 6(b). As Eq. (27), Eq. (36) can be introduced into the scheme (19) by setting $d_{i,j,k} = \tilde{d}_{i,j,k}$ or used to directly update the level set function by $\phi_{i,j,k} = \tilde{d}_{i,j,k}$. Similar to CR-1 a 2-step correction scheme is obtained with Eq. (20) applied in the first step and subsequently Eq. (36) used in the second step. As in CR-1, both steps are performed only once and sequentially such that no iterations between the two steps are necessary to obtain an estimate of $d_{i,j,k}$ on cells at the zero level set. Using the subsets defined in Eq. (28), the scheme CR-2 can hence be summarized as follows:

Step 1. Compute the signed distance function on all cells in $\mathcal{R}$ using Eqs. (20) and (21).
Step 2. Apply Eq. (36) and set $d_{i,j,k} = \tilde{d}_{i,j,k}$ on all cells in $\mathcal{C}$.
Step 3. Update $\phi_{i,j,k} = d_{i,j,k}$ on all cells in Γ.
Step 4. Solve Eq. (29) to steady state on $C_{i,j,k} \in \{\mathcal{B} \setminus \Gamma\}$.

Note the scheme holds for arbitrary $M_{i,j,k}$ even though the derivation above cannot be illustrated geometrically if the cell centers of $\mathcal{S}_{i,j,k}$ are not located within the same plane, which is the case for $M_{i,j,k} > d$, where d is the number of space dimensions.

3.1.3. Discussion of CR-1 and CR-2

The displacement of the zero level set caused by the constrained reinitialization scheme is independent of the number of iterations performed to solve the reinitialization equation. The formulations CR-1 and CR-2 differ in step 2, while steps 1, 3 and 4 are alike. Steps 3 and 4 can be replaced by solving Eq. (19) using the first-order upwind discretization given above with $d_{i,j,k}$ computed in steps 1 and 2. This yields the same accuracy.

Referring to CR-1, Eq. (27) can be generally reformulated to give a correction $\Delta d_{i,j,k}$ of $d_{i,j,k}$, provided $d_{i,j,k}$ has been computed using Eqs. (20) and (21), i.e., the first step is executed on all cells in Γ. Obviously, this yields exactly the same result as the procedure described above.

A further modification is to distribute the correction term to $C_{i,j,k}$ and $\mathcal{S}_{i,j,k}$, such that the corrections $\frac{1}{M_{i,j,k}+1}\Delta d_{i,j,k}$ and $-\frac{1}{M_{i,j,k}+1}\Delta d_{i,j,k}$ are applied to $C_{i,j,k}$ and $\mathcal{S}_{i,j,k}$, respectively. However, numerical tests reveal that this distributed correction procedure produces oscillations and does not improve the accuracy of the proposed scheme.

4. Results

We now turn to present results of numerical experiments using the novel methods. First, the order of the schemes is investigated in a static reinitialization test case, followed by the solid-body rotation of a slotted disk and propagation test cases including topology changes, which are considered to investigate the accuracy and stability of the novel reinitialization schemes.

4.1. Order of the reinitialization schemes

The order of the proposed reinitialization schemes is investigated in a test case similar to that used in [12]. Let the level set function be initialized as

$$\tilde{\phi}(\mathbf{x}) = g(\mathbf{x})(r - \sqrt{x^2 + y^2}), \tag{37a}$$

which defines for $g(\mathbf{x}) = 1$ an infinite number of concentric circular level sets with a zero level set of radius r. Retaining the zero level set, a perturbed level set function with small and large gradients is obtained using

$$g(\mathbf{x}) = 0.1 + (x - r)^2 + (y - r)^2. \tag{37b}$$

Fig. 7 depicts the level set function for $r = 3$ after being reinitialized for a different number of iterations using CR-2 on a 128^2 cell grid. Note, the cells in Γ are updated before the first iteration and remain unchanged thereafter.

To evaluate the order of the different schemes, the L_1 norm of the difference e_1 between the exact signed distance function and the computed function is determined at the zero level set by

$$e_1 = \|D - \phi\|_1 = \frac{1}{\mathcal{N}_\Gamma} \sum_{\Gamma} |D_{i,j} - \phi_{i,j}|, \tag{38}$$

where $D_{i,j} = r - \sqrt{x_{i,j}^2 + y_{i,j}^2}$ is the exact signed distance function and $\mathcal{N}_\Gamma$ denotes the number of cells in Γ. The results are summarized in Tables 1 and 2 and plotted in Fig. 8. As expected, all schemes are second-order accurate at the zero level set. The results furthermore indicate a similar performance of the reinitialization schemes RSU, CR-1 and CR-2 for this problem, which, however, is an artifact of the test case since the initial perturbed level set function is distributed very smoothly. The significantly enhanced accuracy and stability of the constrained reinitialization schemes is demonstrated in Section 4.2, where level set advection and propagation test cases are presented.

4.2. Advection and propagation test cases

In this section solutions of numerical experiments showing the stability and the enhanced accuracy of the novel methods are discussed. For all computations the localized level set method is used. The narrow band $\mathcal{B}$ extends seven cells on each side of the zero level set. Solutions on wider bands have been computed. They show that all presented solutions are almost independent of the bandwidth. The level set function is reinitialized after each time step and Eq. (29) is converged to machine accuracy. The purpose is to demonstrate the stability and enhanced accuracy of the proposed methods even when the reinitialization is performed very frequently and that the reinitialization procedure is independent of the number of iterations performed on Eq. (29). Note, $\mathcal{O}(1)$–$\mathcal{O}(10)$ iterations are usually sufficient to solve Eq. (29) when the level set function is reinitialized after each time step.

4.2.1. Problem 1: rotation of a slotted disk

First, the rotation of a slotted disk [17] is considered. A slot of width 5 and length 25 is cut out of a disk centered at $(x, y) = (50, 75)$ with a radius $r = 15$ in a computational domain $\Omega : [0, 100] \times [0, 100]$. The slotted disk is rotated under a velocity field $(u, v) = (\pi/314(50 - y), \pi/314(x - 50))$, such that a full revolution is performed at $t = 628$. A CFL number of 1.28 is used, which corresponds to a time step $\Delta t = 1$ on a 256^2 cell grid.

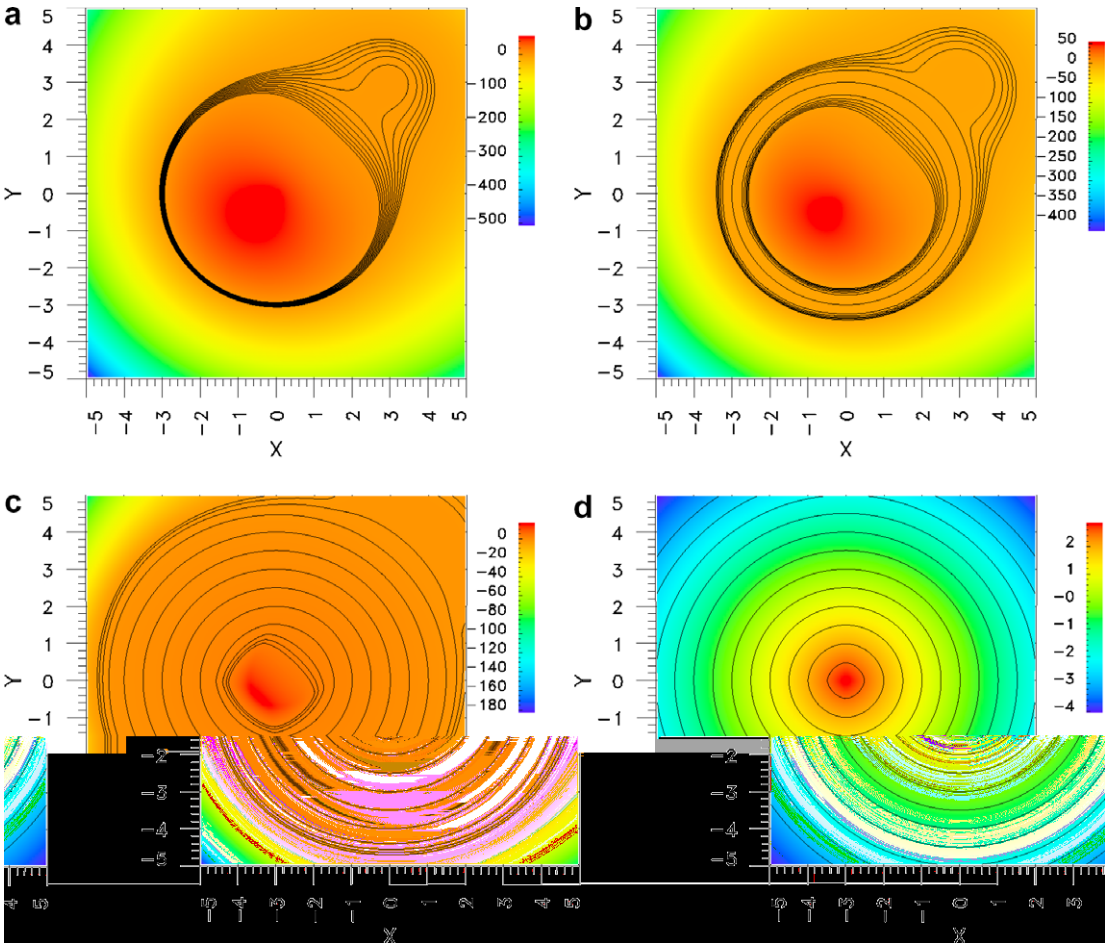

Fig. 7. Reinitialization of the level set function initialized by Eq. (37) into a signed distance function using CR-2 in a computational domain $\Omega : [-5,5] \times [-5,5]$ discretized by 128^2 cells: (a) before the reinitialization; (b) after 10 iterations; (c) after 50 iterations; (d) after 150 iterations. Contours are evenly spaced by 0.5 and plotted in the range $\phi = \{-3,\ldots,3\}$. The colors correspond to the value of the level set function ϕ.

Table 1
Convergence of the reinitialization scheme proposed by Russo and Smereka [12] using different discretizations

Δ_x	e_1: RSC	Order: RSC	e_1: RSU	Order: RSU
10/64	2.000×10^{-3}	–	1.202×10^{-3}	–
10/128	4.958×10^{-4}	2.0	2.974×10^{-4}	2.0
10/256	1.211×10^{-4}	2.0	7.671×10^{-5}	2.0

The level set function is initialized according to Eq. (37).

Table 2
Convergence of the constrained reinitialization schemes CR-1 and CR-2

Δ_x	e_1: CR-1	Order: CR-1	e_1: CR-2	Order: CR-2
10/64	1.273×10^{-3}	–	1.202×10^{-3}	–
10/128	3.060×10^{-4}	2.1	2.863×10^{-4}	2.1
10/256	7.646×10^{-5}	2.0	7.178×10^{-5}	2.0

The level set function is initialized according to Eq. (37).

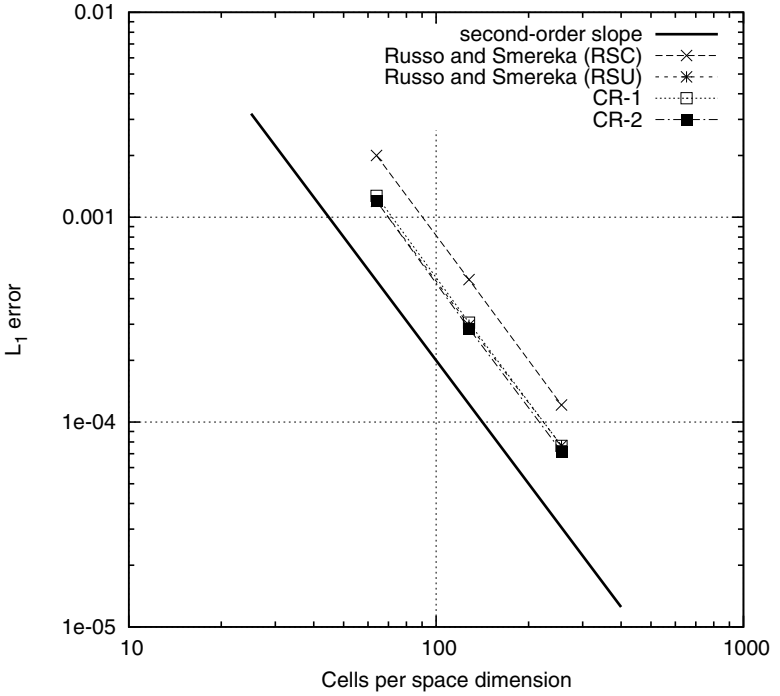

Fig. 8. Convergence of different reinitialization schemes. The level set function is initialized by Eq. (37).

The results using the reinitialization scheme by Russo and Smereka [12] (RSU) and the two formulations CR-1 and CR-2 of the new reinitialization scheme are compared in Figs. 9 and 10, where the solutions after 1, 2 and 3 full revolutions of the slotted disk are plotted. The plots in Figs. 9 and 10 are computed using the third-order accurate spatial and temporal discretization UC_3/RK_3 and the fifth-order accurate spatial and third-order accurate temporal discretization UC_5/RK_3, respectively. The solutions using CR-1 and CR-2 are clearly more accurate than the RSU findings. After 3 revolutions, the slot has almost disappeared in the RSU solutions and a significant area loss of the disk is apparent. In Table 3, the area loss, which is nearly proportional to the number of revolutions, is juxtaposed for the solutions of the different discretization and reinitialization schemes. Using CR-1 and CR-2 and UC_5/RK_3, about 0.3% of the disk area is lost per revolution, whereas the loss is up to 17 times larger in the RSU solutions. In Fig. 11(a), the mean displacement of the zero level set determined by linear interpolation in the x and in the y direction is plotted over time for the UC_5/RK_3 solutions. The displacement caused by CR-1 and CR-2 is roughly an order of magnitude smaller than that by RSU, while Fig. 11(b) evidences the condition $|\nabla\phi| = 1$ to be equally well fulfilled by all schemes for the cells in Γ. The local anchoring of the zero level set in CR-2 provides a similar accuracy as the minimization of the ϕ_0 displacement via the least-squares method being used in CR-1.

Comparing the RSU results of the different discretizations UC_3/RK_3 and UC_5/RK_3 in Figs. 9, 10 and Table 3 yields only a small difference between the solutions despite the considerable difference in the orders of the discretization schemes. The CR-1 and CR-2 solutions, however, clearly improve when UC_5/RK_3 is used instead of UC_3/RK_3 and the area loss is reduced by a factor of 2. Hence, the displacement of the zero level set caused by the RSU reinitialization scheme dominates the higher accuracy of the UC_5/RK_3 discretization, thereby diminishing the quality of the solution. This is an important result, considering the fact that many authors use higher-order methods to discretize the level set equation.

For a further investigation reference solutions have been computed using the reinitialization scheme

$$\begin{cases} \phi_{i,j,k} = \tilde{\phi}_{i,j,k} & \text{if } C_{i,j,k} \in \Gamma, \\ \phi^{v+1}_{i,j,k} = \phi^{v}_{i,j,k} - \Delta\tau \ \mathrm{sgn}(\tilde{\phi}_{i,j,k})(|\nabla\phi^{v}_{i,j,k}| - 1) & \text{otherwise.} \end{cases} \tag{39}$$

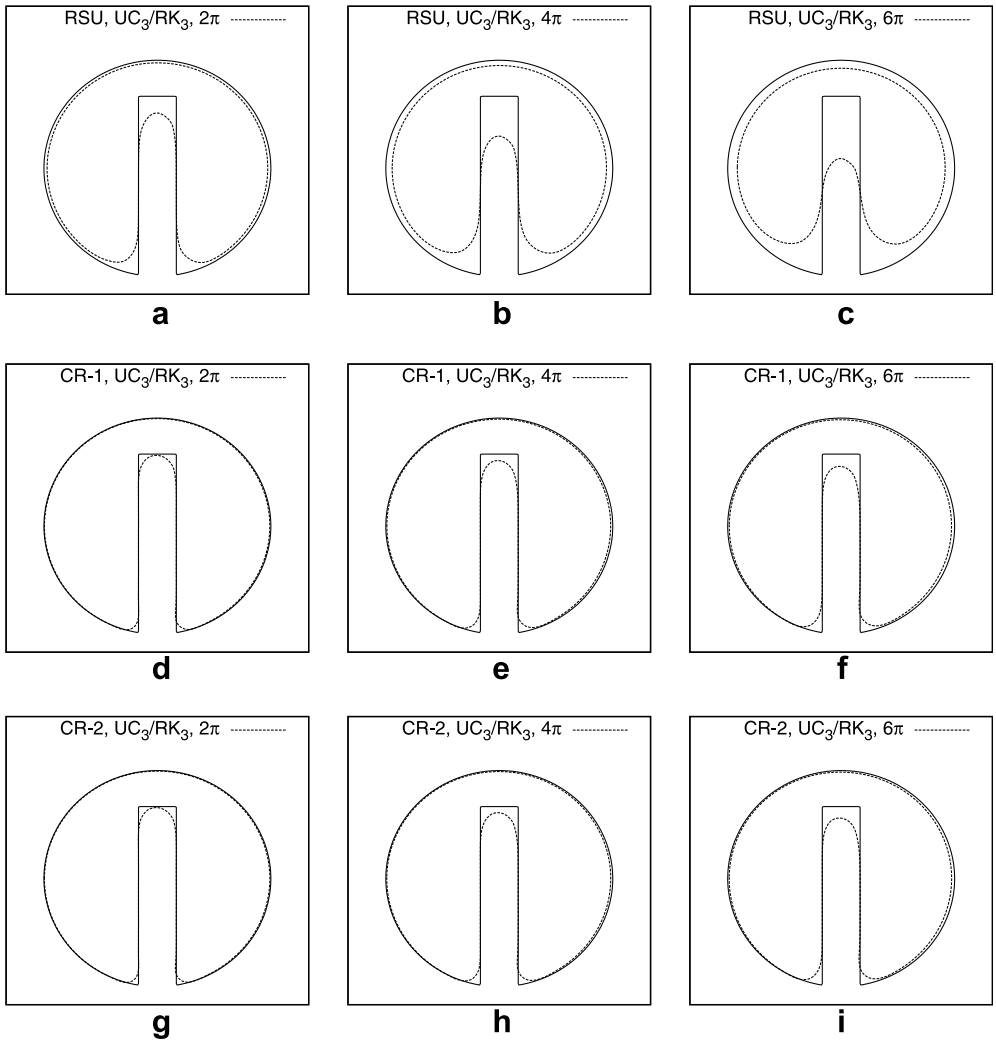

Fig. 9. Problem 1: rotation of a slotted disk using the localized level set method on a 256^2 cell grid. Comparison of different reinitialization schemes: (a–c) RSU; (d–f) CR-1; (g–i) CR-2. UC_3/RK_3 solutions are shown for 1 full revolution (a, d, g), 2 full revolutions (b, e, h) and 3 full revolutions (c, f, i) of the disk.

If the zero level set is recovered by linear interpolation, this scheme exactly preserves the interface but is unable to restore $|\nabla\phi| = 1$ in Γ. Using the solution based on this scheme as reference indicates in how far a different reinitialization scheme is able to improve the solution by approximating $|\nabla\phi| = 1$ in Γ at the cost of moving the zero level set. In Fig. 12, $UC_5/\ RK_3$ solutions with the reinitialization scheme (39) are plotted and compared with the respective solutions using CR-2 as reinitialization scheme, showing the latter to be slightly superior. Unlike the novel constrained reinitialization schemes, the scheme RSU results in a displacement of the zero level set which clearly lowers the benefit of restoring $|\nabla\phi| = 1$ in Γ. This fact is evidenced in Figs. 12 and 9(a)–(c), 10(a)–(c).

Note the reinitialization scheme (39) works rather well for simple displacement and solid body rotation test cases such as the one presented, but is unable to remove the steep and small gradients emerging at the interface in more demanding test cases such as problem 2 presented in Section 4.2.2. For this test case, a localized level set solution could not be obtained using Eq. (39) to reinitialize the level set function.

In [18], Dupont and Liu propose a simple reinitialization strategy based on the reinitialization Eq. (9), which is in the following referred to as DL. A reinitialization of the level set function is performed after each

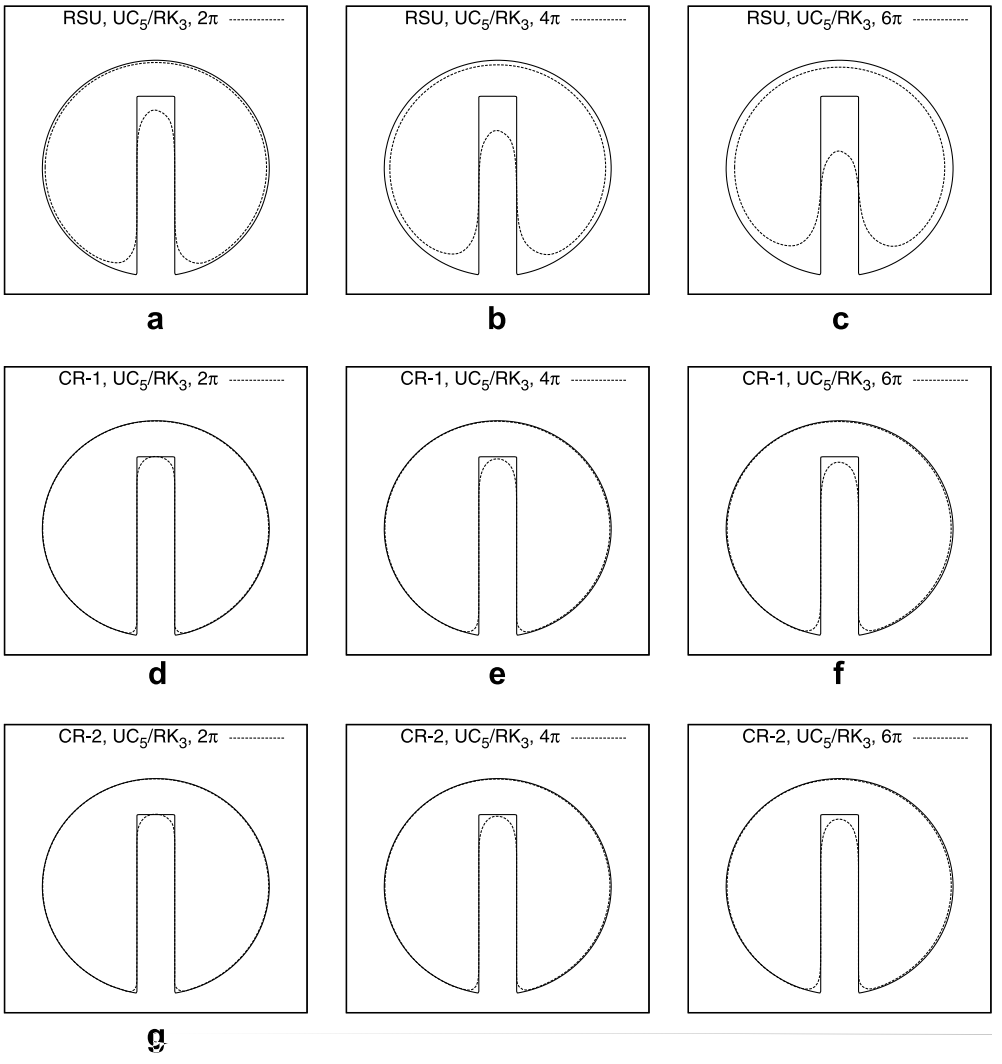

level set time step and Eq. (9) is solved only on certain cells which satisfy specific conditions. These conditions are verified after each pseudo-time step v. Given a solution ϕ^v after v iterations of Eq. (9), ϕ^{v+1} is only computed on cells $C_{i,j,k}$ for which either $\Pi^{i,j,k}_{\hat{i},\hat{j},\hat{k}}\phi^v > 0$ for all integers $\hat{i},\hat{j},\hat{k}$ satisfying $|\hat{i}-i| \leqslant 1$, $|\hat{j}-j| \leqslant 1$ and $|\hat{k}-k| \leqslant 1$, or

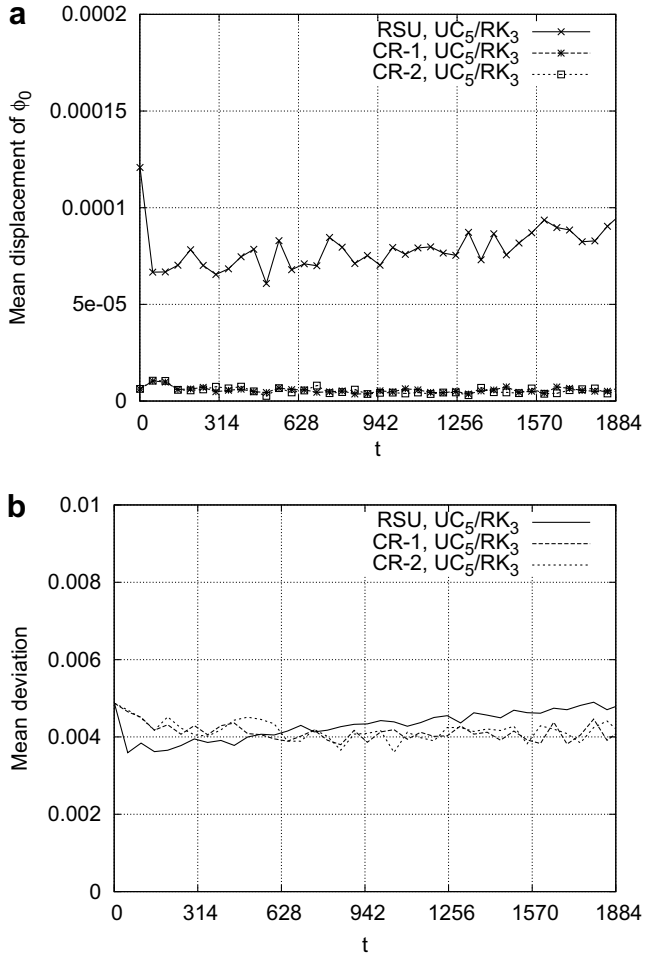

Fig. 11. Comparison of different reinitialization schemes for problem 1 illustrated in Fig. 10: (a) mean displacement of the zero level set within the reinitialization; (b) mean deviation from $|\nabla\phi| = 1$ on cells in Γ. The data is plotted for each 50th time step for a total of three revolutions of the disk.

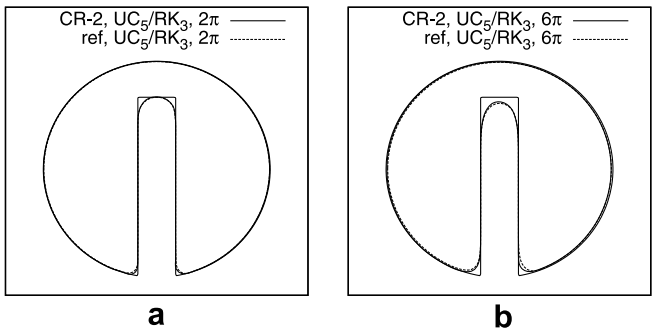

Fig. 12. Comparison between solutions of CR-2 and the reference scheme given by Eq. (39) for problem 1, see Fig. 10: (a) after 1 revolution; (b) after 3 revolutions. Solutions with CR-2 correspond to those plotted in Fig. 10(g and i), respectively.

$$|\phi^v_{i,j,k} - \phi^v_{i',j,k}| > 1.1\Delta_{\mathbf{x}} \vee |\phi^v_{i,j,k} - \phi^v_{i,j',k}| > 1.1\Delta_{\mathbf{x}} \vee |\phi^v_{i,j,k} - \phi^v_{i,j,k'}| > 1.1\Delta_{\mathbf{x}} \tag{40}$$

for any integer $i' \in \{i+1, i-1\}, j' \in \{j+1, j-1\}, k' \in \{k+1, k-1\}$. On all other cells ϕ^{v+1} is set $\phi^{v+1} = \phi^v$.

Like the schemes RSU, CR-1 and CR-2 Eq. (9) is converged to machine accuracy and discretized by the first-order upwind scheme (29). It is clear that, unlike RSU and the novel schemes CR-1 and CR-2, the unwanted displacement of the zero level set depends on the number of iterations that are performed to solve Eq. (9).

Let us briefly revisit the test case investigated in Section 4.1. The DL results for this test case are summarized in Table 4 and juxtaposed with the CR-1 and CR-2 results from Table 2. The DL scheme is first-order accurate and produces an error e_1 which is roughly two orders of magnitude larger than that of CR-2 for the investigated grids. The reason is that DL becomes inaccurate when the gradients at ϕ_0 are steep requiring several iterations of Eq. (9) on cells in Γ as long as the condition (40) is satisfied. This results in the unwanted displacement of the zero level set.

For the rotation of a slotted disk on a 256^2 cell grid, the DL scheme gives excellent results and the solutions are superior to those obtained with CR-2, as shown in Fig. 13. This can be explained as follows. First of all, excellent results for the rotation of a slotted disk can be obtained without reinitialization, which is why the rotation of a slotted disk is primarily a good test case to assess solution methods for the level set equation. One of the challenges of this test case is that the reinitialization procedure tends to smooth out the corners of the slotted disk. The DL scheme overcomes this problem to some extent since its formulation means for this particular test case that the level set function is rarely reinitialized on the cells near the level set front. However, referring to the results presented in Table 4, unlike the novel constrained reinitialization schemes the accuracy of the DL scheme is substantially diminished as soon as steep gradients are present near the level set front requiring several iterations of the reinitialization Eq. (9) on the cells in this region. This is one of the reasons leading to the failure of the method in the test case presented in Section 4.2.2.

Finally, solutions on a finer 512^2 cell grid using the 256^2 cell grid CFL number 1.28, i.e., a time step of $\Delta t = 0.5$ is prescribed, are presented. Due to the smaller time step, twice as many reinitialization steps are performed in the fine grid simulations as in the coarse grid simulations. In Fig. 14, the solutions after 1 disk revolution obtained on a grid with mesh spacing $\Delta_{\mathbf{x}} = \frac{100}{512}$ using CR-2 are plotted. Table 5 gives the area loss for the different discretization and reinitialization schemes. The fine-grid solutions corroborate the conclusions drawn from the coarse-grid results.

Table 4
Comparison of CR-1, CR-2 and DL in the reinitialization test case presented in Section 4.1

$\Delta_{\mathbf{x}}$	e_1: CR-1	e_1: CR-2	e_1: DL	Order: DL
10/64	1.273×10^{-3}	1.202×10^{-3}	2.023×10^{-2}	–
10/128	3.060×10^{-4}	2.863×10^{-4}	9.075×10^{-3}	1.16
10/256	7.646×10^{-5}	7.178×10^{-5}	4.630×10^{-3}	0.97

The level set function is initialized according to Eq. (37).

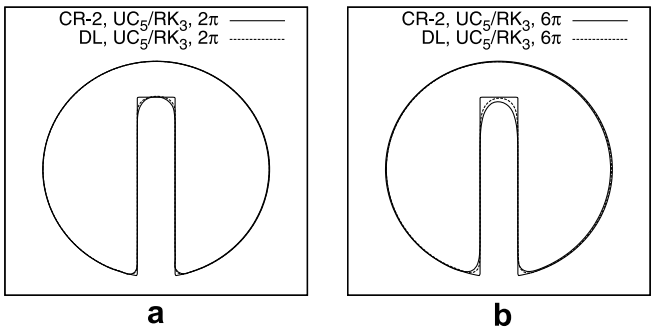

Fig. 13. Comparison between CR-2 and DL solutions for problem 1, see Fig. 10: (a) after 1 revolution; (b) after 3 revolutions. Solutions with CR-2 correspond to those plotted in Fig. 10(g and i), respectively.

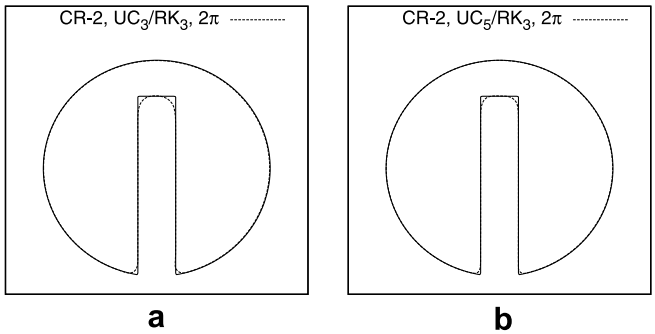

Fig. 14. Problem 1: rotation of a slotted disk using the localized level set method on a 512^2 cell grid. Comparison of different discretization schemes: (a) UC_3/RK_3; (b) UC_5/RK_3.

Table 5
Problem 1: rotation of a slotted disk

Time t (Revolutions)	UC_3/RK_3 (%)			UC_5/RK_3 (%)		
	RSU	CR-1	CR-2	RSU	CR-1	CR-2
628 (1)	2.50	0.29	0.27	2.27	0.15	0.14
1256 (2)	5.11	0.60	0.57	4.62	0.30	0.29
1884 (3)	7.77	0.92	0.87	7.01	0.45	0.43

Comparison of the area loss after 1, 2 and 3 revolutions of the slotted disk between solutions of several reinitialization schemes on a 512^2 cell grid.

4.2.2. Problem 2: oscillating circle

Next, results of a level set propagation test case are discussed, in which the propagation speed is a function of space and time as in many physical applications of level set methods such as in turbulent premixed combustion. A circular interface with radius $r = 3$ centered at $(x, y) = (0, 0)$ in a computational domain $\Omega : [-5, 5] \times [-5, 5]$ is considered and the speed of propagation s normal to the zero level set is defined by

$$s = \cos(8\Theta)\sin(\omega), \tag{41a}$$

where

$$\Theta = \arctan\left|\frac{y}{x}\right|, \quad \omega = \frac{2\pi t}{t_e}. \tag{41b}$$

The time step is $\Delta t = \frac{\Delta x}{4}$ corresponding to a CFL number of 0.25 and $t_e = 5$ is used on all grids. The extension velocity $\mathbf{f} = s\mathbf{n}$ is prescribed on the cells in Γ and determined in Ω_ϕ using the method described in [13].

In Fig. 15, the zero level set is plotted at $\omega = \pi$, $\omega = 2\pi$ and $\omega = 6\pi$ for UC_5/RK_3 solutions obtained on a 256^2 cell grid. The different reinitialization schemes RSU, CR-1 and CR-2 are compared. Qualitatively, CR-1 and CR-2 give a significantly improved solution compared to RSU. In Fig. 16, the solutions obtained using CR-2 and DL on different grids are compared. Using the DL reinitialization scheme, the original circular shape of the zero level set is not attained at $\omega = 2\pi$ and artifacts of the oscillatory motion are clearly visible. These artifacts emerge primarily when the zero level set is contracted to its original circular shape, as the plots in Fig. 16 illustrate. However, Fig. 16(a) shows that the DL solution exhibits small instabilities already at $\omega = \pi$ on the 128^2 cell grid. The reason for the failure of the DL scheme in this test case is twofold: (1) the DL scheme is unable to correct the level set function on cells in Γ where ϕ is flat, i.e. $0 < |\nabla\phi| < 1$; (2) as discussed in Section 4.2.1, the DL scheme is able to remove steep gradients on cells in Γ, but at the cost of moving the zero level set considerably. In [18], the DL scheme is used with only two iterations of Eq. (9) per reinitialization step, which, however, does not significantly improve the DL solution of the oscillating circle problem. In Table 6, the area loss is listed for the RSU, CR-1 and CR-2 solutions at $\omega = 2\pi$. Using CR-1 and CR-2, area is gained, and the area defect is reduced by a factor of roughly 20 compared with the RSU findings. The

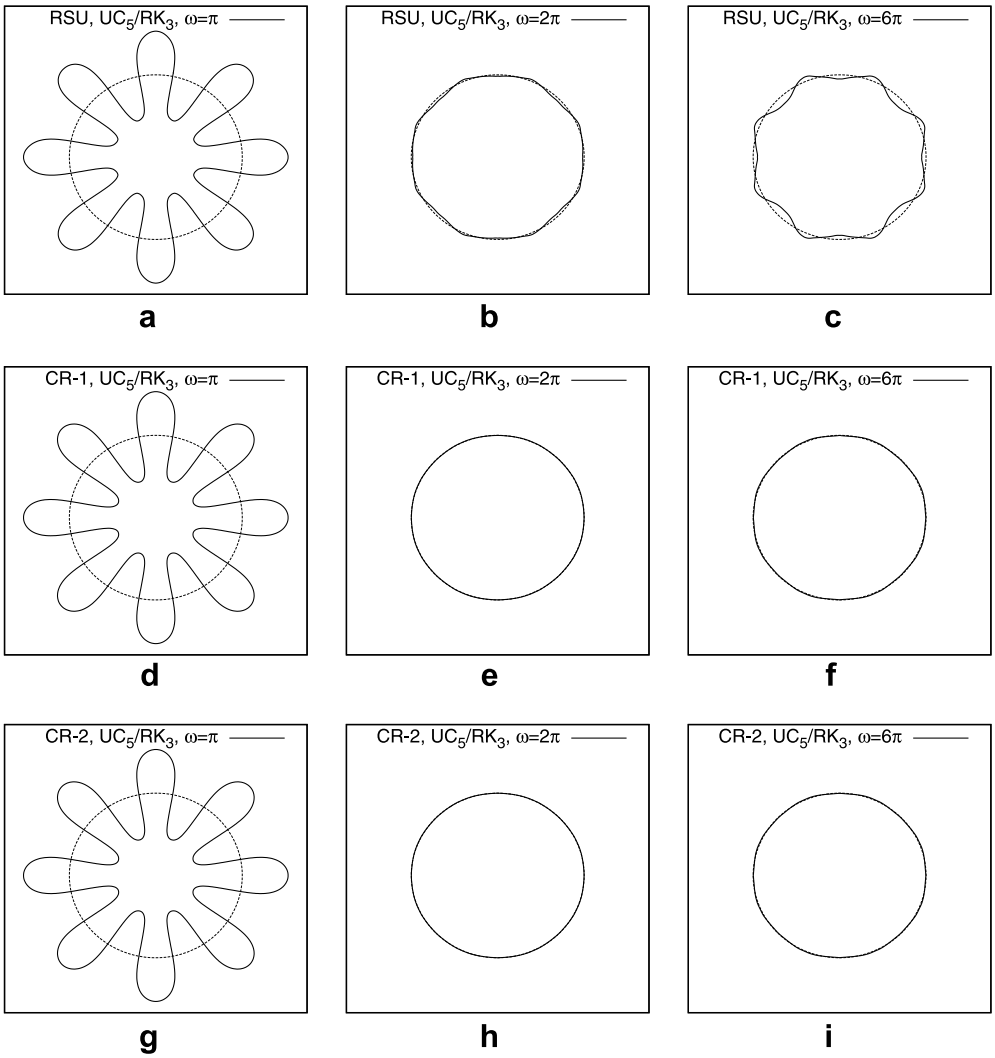

Fig. 15. Problem 2: propagation of a circle with space- and time-dependent speed using the localized level set method on a 256^2 cell grid. Comparison of different reinitialization schemes: (a–c) RSU; (d–f) CR-1; (g–i) CR-2. UC_5/RK_3 solutions are shown at $\omega = \pi$ (a, d, g), $\omega = 2\pi$ (b,e,h) and $\omega = 6\pi$ (c, f, i), respectively. Dashed lines: initial zero level set.

rate at which the area defect decreases with increasing grid refinement is approximately first order for all schemes.

In Fig. 17, the mean displacement of the zero level set within the reinitialization and the mean deviation from $|\nabla\phi| = 1$ are plotted for the different reinitialization schemes showing essentially the same trend as for problem 1. An interesting feature of the schemes CR-1 and CR-2 is highlighted by Fig. 17(a) indicating that the displacement of the zero level set within the reinitialization goes to zero as the propagation speed goes to zero, i.e., at $\omega = \{0, \pi, 2\pi\}$. Clearly, this is not the case for RSU.

4.2.3. Problem 3: topology changes

Finally, results of numerical simulations of coalescing and segregating interfaces obtained by the novel schemes are briefly presented. The initial level set function is given by

$$\phi(\mathbf{x}) = \min\left(r - \sqrt{(x-a)^2 + y^2}, r - \sqrt{(x+a)^2 + y^2}\right), \tag{42}$$

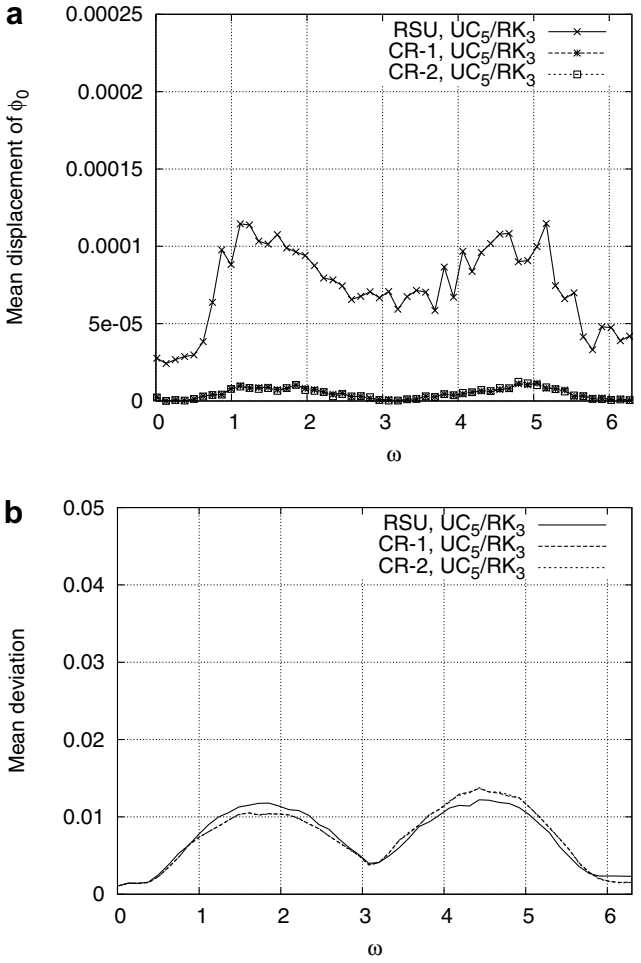

Fig. 17. Comparison of different reinitialization schemes for problem 2 illustrated in Fig. 15: (a) mean displacement of the zero level set within the reinitialization; (b) mean deviation from $|\nabla\phi| = 1$ on cells in Γ. The data is plotted for each 10th time step.

$$H(s) = \begin{cases} s & \text{if } t < 1.0, \\ -s & \text{otherwise}, \end{cases} \tag{43}$$

which is prescribed on the cells in Γ. Using $s = 1$ and a CFL number of 0.064 gives a time step of $\Delta t = 0.005$. This rather small CFL number is used to highlight the difference between the reinitialization schemes and the accuracy of the proposed methods for small time steps and correspondingly a large number of reinitialization steps. The solution is run until $t = 3.2$. As for problem 2, the extension velocity is extended in Ω_ϕ before each time step using the method proposed in [13]. In Fig. 18, the solution is plotted for the reinitialization schemes RSU and CR-2 at different time levels showing the two circular zero level sets being coalesced and segregated. In Fig. 18(g) and (h) the analytically exact solution is given as reference, indicating the enhanced accuracy of CR-2 compared to RSU, although the difference between both solutions is rather small up to $t = 1.2$ since the circular interfaces are essentially uniformly expanded and shrunk. Solutions obtained with CR-1 (not shown) are indistinguishable from those obtained with CR-2. As in problem 1, the sharp corners of the interface are smoothed in the level set solutions hence, the interface segregation occurs at a later time, which becomes apparent when Fig. 18(a) and (f), (b) and (e), and (c) and (d) are compared.

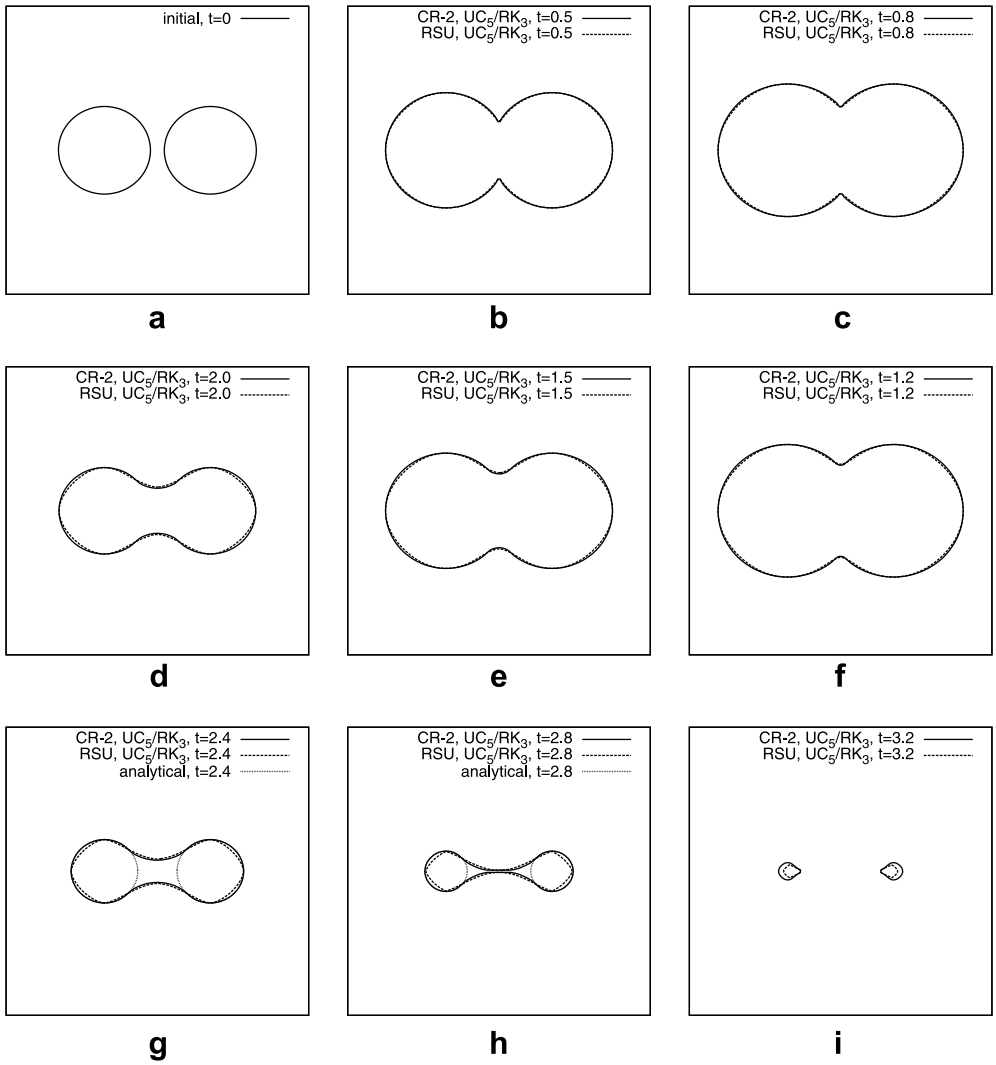

Fig. 18. Problem 3: coalescing and segregating interfaces using the localized level set method on a 128^2 cell grid. Comparison of the reinitialization schemes RSU and CR-2. The analytically exact solution is given as reference in (g) and (h). UC_5/RK_3 solutions are plotted at (a) $t = 0$, (b) $t = 0.5$, (c) $t = 0.8$, (d) $t = 1.2$, (e) $t = 1.5$, (f) $t = 2.0$, (g) $t = 2.4$, (h) $t = 2.8$, (i) $t = 3.2$. To more easily compare (c) and (d), (b) and (e) and (a) and (f) the center row is to be read from right to left.

5. Summary

Two formulations of a new partial differential equation based reinitialization scheme have been derived in the framework of a localized level set method. The new reinitialization scheme takes the location of the interface explicitly into account. The first formulation is derived using the least-squares method to minimize the displacement of the interface within the reinitialization. The second formulation is derived by reducing the overdetermined problem, which is solved in the first formulation, to a determined one. It is shown that the resulting scheme locally preserves the location of the interface. Both formulations result in algorithms that are simple to implement and computationally efficient.

The enhanced accuracy and the stability of the proposed methods are evidenced by numerical simulations of the rotation of a slotted disk, a propagation test case relevant for the application of level set methods in turbulent premixed combustion and an interface coalescing and segregating problem. It is demonstrated that the accuracy of high-order discretizations of the level set equation is preserved even when the level set function

is reinitialized after each time step. The proposed methods can be efficiently applied to localized and global level set methods. From the findings of the test cases it can be concluded the second formulation to be slightly more accurate than the first formulation. Both methods outperform the existing schemes, which have been used as reference forms, with respect to accuracy and robustness, i.e., the susceptibility to the discretization scheme and the number of reinitialization steps.

Acknowledgments

This research is part of the collaborative research center SFB 686 which is funded by the German Research Association (Deutsche Forschungsgemeinschaft (DFG)). The support of the DFG is gratefully acknowledged.

References

[1] N. Peters, Turbulent Combustion, Cambridge University Press, 2000.
[2] H. Pitsch, A consistent level set formulation for large-eddy simulation of premixed turbulent combustion, Combust. Flame 143 (2005) 587–598.
[3] M. Sussman, K. Smith, M. Hussaini, M. Ohta, R. Zhi-Wei, A sharp interface method for incompressible two-phase flows, J. Comput. Phys. 221 (2007) 469–505.
[4] M. Sussman, A. Almgren, J. Bell, P. Colella, L. Howell, M. Welcome, An adaptive level set approach for incompressible two-phase flows, J. Comput. Phys. 148 (1999) 81–124.
[5] F. Gibou, R. Fedkiw, R. Caflisch, S. Osher, A level set approach for the numerical simulation of dendritic growth, J. Sci. Comput. 19 (2003) 183–199.
[6] G. Markstein, Nonsteady Flame Propagation, Pergamon Press, 1964.
[7] S. Osher, J. Sethian, Fronts propagating with curvature-dependent speed: algorithms based on Hamilton–Jacobi formulations, J. Comput. Phys. 79 (1988) 12–49.
[8] R. Nourgaliev, T. Theofanous, High-fidelity interface tracking in compressible flows: unlimited anchored adaptive level set, J. Comput. Phys. 224 (2007) 836–866.
[9] G.-S. Jiang, D. Peng, Weighted ENO schemes for Hamilton–Jacobi equations, SIAM J. Sci. Comput. 21 (2000) 2126–2143.
[10] M. Sussman, P. Smereka, S. Osher, A level set approach for computing solutions to incompressible two-phase flow, J. Comput. Phys. 114 (1994) 146–159.
[11] B. Merriman, J. Bence, S. Osher, Motion of multiple junctions: a level set approach, J. Comput. Phys. 112 (1994) 334–363.
[12] G. Russo, P. Smereka, A remark on computing distance functions, J. Comput. Phys. 163 (2000) 51–67.
[13] D. Peng, B. Merriman, S. Osher, H. Zhao, M. Kang, A PDE-based fast local level set method, J. Comput. Phys. 155 (1999) 410–438.
[14] D. Adalsteinsson, J. Sethian, A fast level set method for propagating interfaces, J. Comput. Phys. 118 (1995) 269–277.
[15] D. Hartmann, M. Meinke, W. Schröder, An adaptive multilevel multigrid formulation for Cartesian hierarchical grid methods, Comput. Fluids, in press, doi:10.1016/j.compfluid.2007.06.007.
[16] C.-W. Shu, S. Osher, Efficient implementation of essentially non-oscillatory shock-capturing schemes, J. Comput. Phys. 77 (1988) 439–471.
[17] S. Zalesak, Fully multidimensional flux-corrected transport algorithms for fluids, J. Comput. Phys. 31 (1979) 335–362.
[18] T. Dupont, Y. Liu, Back and forth error compensation and correction methods for semi-Lagrangian schemes with application to level set interface computations, Math. Comput. 76 (2007) 647–668.